CrossMark

AMERICAN ACADEMY OF OPHTHALMOLOGY
The Eye M.D. Association

The Onion Sign in Neovascular Age-Related Macular Degeneration Represents Cholesterol Crystals

Claudine E. Pang, MD,[1] *Jeffrey D. Messinger, DC,*[3] *Emma C. Zanzottera, MD,*[3,4] *K. Bailey Freund, MD,*[1,2,5] *Christine A. Curcio, PhD*[3]

Purpose: To investigate the frequency, natural evolution, and histologic correlates of layered, hyperreflective, subretinal pigment epithelium (sub-RPE) lines, known as the onion sign, in neovascular age-related macular degeneration (AMD).

Design: Retrospective observational cohort study and experimental laboratory study.

Participants: Two hundred thirty eyes of 150 consecutive patients with neovascular AMD and 40 human donor eyes with histopathologic diagnosis of neovascular AMD.

Methods: Spectral-domain optical coherence tomography (SD OCT), near-infrared reflectance (NIR), color fundus images, and medical charts were reviewed. Donor eyes underwent multimodal ex vivo imaging, including SD OCT, before processing for high-resolution histologic analysis.

Main Outcome Measures: Presence of layered, hyperreflective sub-RPE lines, qualitative analysis of their change in appearance over time with SD OCT, histologic correlates of these lines, and associated findings within surrounding tissues.

Results: Sixteen of 230 eyes of patients (7.0%) and 2 of 40 donor eyes (5.0%) with neovascular AMD had layered, hyperreflective sub-RPE lines on SD OCT imaging. These appeared as refractile, yellow-gray exudates on color imaging and as hyperreflective lesions on NIR. In all 16 patient eyes, the onion sign persisted in follow-up for up to 5 years, with fluctuations in the abundance of lines and association with intraretinal hyperreflective foci. Patients with the onion sign disproportionately were taking cholesterol-lowering medications ($P = 0.025$). Histologic analysis of 2 donor eyes revealed that the hyperreflective lines correlated with clefts created by extraction of cholesterol crystals during tissue processing. The fluid surrounding the crystals contained lipid, yet was distinct from oily drusen. Intraretinal hyperreflective foci correlated with intraretinal RPE and lipid-filled cells of probable monocytic origin.

Conclusions: Persistent and dynamic, the onion sign represents sub-RPE cholesterol crystal precipitation in an aqueous environment. The frequency of the onion sign in neovascular AMD in a referral practice and a pathology archive is 5% to 7%. Associations include use of cholesterol-lowering medication and intraretinal hyperreflective foci attributable to RPE cells and lipid-filled cells of monocyte origin. *Ophthalmology 2015;122:2316-2326 © 2015 by the American Academy of Ophthalmology.*

Supplemental material is available at www.aaojournal.org.

The onion sign was first described by Mukkamala et al[1] as a novel spectral-domain (SD) optical coherence tomography (OCT) finding of layered hyperreflective lines beneath the retinal pigment epithelium (RPE) (the sub-RPE space) usually associated with chronic exudation from type 1 neovascularization in patients with age-related macular degeneration (AMD). Typically associated with intense signal on near-infrared reflectance (NIR) scanning laser ophthalmoscopy (SLO), the onion sign was proposed by its discoverers to represent layers of precipitated lipid amidst chronic exudation[1,2] after also considering collagen or fibrin.[1] Others authors suggested fibrovascular scarring,[3] mechanical strain on Bruch's membrane, and dystrophic calcification in drusen regression[4,5] as possible histologic correlates.

Independently, Christakopoulos et al[6] hypothesized that hyperreflective lines in the onion sign represent cholesterol crystals, because they are transparent and not associated with shadowing, like calcification. This hypothesis is credible because cholesterol crystals appear as linear, highly reflecting structures in atherosclerotic coronary artery plaques viewed by SD OCT[7] in which reflections are generated from interfaces between crystal surfaces and surrounding tissue. This designation for cardiovascular disease was validated in autopsy and endarterial specimens analyzed by ex vivo OCT and subsequent

http://dx.doi.org/10.1016/j.ophtha.2015.07.008
ISSN 0161-6420/15

histologic analysis.[8,9] Tissue processing using ethanol dissolves crystals, leaving distinctive lucent clefts.[10] In human eye pathologic conditions, clefts have been reported within 1 disciform scar secondary to AMD,[11] yet not in aged and early AMD eyes, which have cholesterol-rich lipoprotein deposits in drusen and Bruch's membrane.[12]

Our goals were to document the frequency and natural history of the onion sign in AMD patients and to resolve the controversy behind the hyperreflective material with histologic analysis of 2 cases identified among archival donor eyes by ex vivo SD OCT. By confirming the cholesterol crystal hypothesis, our data reinforced the potential synergy of in vivo SD OCT, ex vivo SD OCT, and histologic analysis for molecular discovery. This information is valuable to clinicians because it aids in the understanding of pathophysiology underlying AMD as well as informing diagnosis and therapeutic decision making.

Methods

The Western Institutional Review Board and the Institutional Review Board at University of Alabama at Birmingham approved the retrospective, observational cohort study and the experimental study, respectively. Research complied with the Health Insurance Portability and Accountability Act and adhered to the tenets of the Declaration of Helsinki.

Retrospective Observational Cohort Study

Medical billing records from March 15, 2014, through September 15, 2014, were used to identify consecutive patients seen by a single physician (K.B.F.) in a vitreoretinal referral practice located in New York, New York, with a diagnosis code 362.52 for neovascular AMD in the International Statistical Classification of Diseases and Related Health Problems, 9th Revision. All patients had received anti−vascular endothelial growth factor (VEGF) therapy within the course of follow-up, although this was not an inclusion requirement. All patient medical charts, color fundus photography obtained with the TRC 50DX retinal camera (Topcon Corporation, Tokyo, Japan), SD OCT images, and simultaneous NIR SLO images with a light stimulus of 815 nm obtained with the Spectralis (Heidelberg Engineering, Heidelberg, Germany) were reviewed. The onion sign was identified as the presence of layered, hyperreflective sub-RPE bands with SD OCT imaging and correlated with findings on color fundus photography and NIR SLO imaging. Serial eye-tracked SD OCT scans were used to perform qualitative analysis of the onion sign from the time of first detection to the most recent visit. The SD OCT scanning protocol used in all eyes comprised parallel horizontal line scans over the area of interest, each scan spaced approximately 150 to 250 μm apart, with automatic real-time averaging set between 16 and 32. The abundance of lines within the onion sign was considered to be increased if the number or the lengths of hyperreflective lines increased and decreased if numbers or lengths decreased.

To investigate the possibility of an association of the onion sign with systemic hypercholesterolemia, the use of an oral cholesterol-lowering medication was recorded. The association of medication use with the occurrence of the onion sign was assessed for statistical significance using the Fisher exact test and SPSS software version 22.0 (IBM Corporation, Armonk, NY). A P value less than 0.05 was accepted as significant.

Histopathologic Study

Neovascular AMD eyes were identified through an ex vivo imaging screen of eyes accessioned for research purposes from nondiabetic white donors to the Alabama Eye Bank from 1996 through 2012. Median death-to-preservation time was 3 hours and 49 minutes (range, 40 minutes−11 hours and 40 minutes). Eyes were preserved by immersion in 1% paraformaldehyde and 2.5% glutaraldehyde in 0.1-M phosphate buffer after anterior segment excision. After removal of vitreous, maculae were photographed in color on a stereomicroscope (SMZ-U; Nikon, Melville, NY), using 35-mm color film (1996−2005) or a digital camera (CoolPix [Nikon]; 2005−2009). For both image formats, pigmentary changes were accentuated with oblique transillumination via a dark-field base, and drusen were accentuated using epi-illumination via a ring light affixed to the objective of the dissecting scope. Eyes underwent additional multimodal ex vivo imaging, including SD OCT, when prepared for histologic analysis (2011−2013). From each globe, an 8-mm-diameter full-thickness tissue punch containing the fovea and temporal portion of the optic nerve head was removed with a trephine. This punch was held in a tissue holder (courtesy of J. Fischer, Heidelberg Engineering) mounted on a Spectralis device (Supplementary material, available at www.aaojournal.org). The holder was a closed chamber with a 60-diopter lens in the front (facing into the SD OCT instrument) and a slot to hold the tissue, with the inner limiting membrane facing forward, in the back. Using tissues stabilized in this manner, we performed a 30°×20° SD OCT volume (143 scans, 30-μm spacing, with automatic real-time set at 25) and red-free SLO. Ex vivo SD OCT differs distinctly from its in vivo counterpart, yet is interpretable with experience. Postmortem edema overall reduces contrast in the neurosensory retina and underlying choroid.[13] The RPE−Bruch's membrane band usually is visible. The 2 synaptic layers, photoreceptor ellipsoid zone, and choroidal vessels also are visible in the best-preserved specimens. Fluid is hyporeflective. Eyes also underwent NIR SLO and autofluorescence SLO with excitation wavelengths of 488 nm for lipofuscin-melanolipofuscin and 787 nm for melanosomes.

Macular tissue punches were postfixed by osmium tannic acid paraphenylenediamine to accentuate extracellular lipid and were embedded in epoxy resin (PolyBed 812; Polysciences, Warrington, PA).[14] Submicrometer-thick sections were stained with 1% toluidine blue and were reviewed and photodocumented with a ×60 oil-immersion objective (numerical aperture, 1.4) and digital camera (XC10 [Olympus, Center Valley, PA]; ×1900 viewing magnification on a monitor). Histologic sections were annotated and uploaded to the Project MACULA online digital microscope (available at project-macula.cis.uab.edu). Forty eyes of 40 donors (25 women with a mean age of 86.9±5.9 years and 15 men with a mean age of 82.2±7.3 years) had neovascular AMD, defined by fibrovascular scarring in the presence of severe RPE change plus drusen, basal linear deposits (BLinD), or both.[15] Two neovascular AMD eyes exhibiting highly hyperreflective lines in the sub-RPE compartment consistent with the onion sign were identified. We used the nomenclature of Staurenghi et al[16] for SD OCT bands and that of Zanzottera et al[17] for RPE morphologic features in histologic examination.

Results

Clinical Imaging and Associations

A cohort of 230 eyes of 150 consecutive patients (mean age, 84 years; 108 women and 42 men) with neovascular AMD was identified. Of these, 16 eyes of 15 patients (7.0%; mean age,

82 years; 13 women and 2 men) were found to exhibit the onion sign with SD OCT imaging. The onion sign corresponded to refractile yellow-gray exudates on color fundus photography and hyperreflective lesions on NIR SLO imaging in all 16 eyes (Fig 1).

Qualitative analysis of serial SD OCT scans revealed that the onion sign persisted in all 16 eyes over the follow-up duration (mean, 3.7 years; range, 0.5−5 years). Fluctuations in the appearance of the onion sign were noted, with 13 eyes exhibiting decreased abundance of lines and 3 eyes showing increased abundance of lines over the follow-up period. In addition, all 16 eyes with the onion sign were found to have adjacent areas of multiple intraretinal hyperreflective foci with SD OCT imaging (Fig 2).

Of the 135 patients without the onion sign, 54 patients (40%) reported using oral cholesterol-lowering medication. This rate was consistent with the percentage of United States adults reporting use of these agents (range, 39.1%−54.4%[18]). Of the 15 patients with the onion sign, 11 patients (73%) were using cholesterol-lowering medications. This association was significant ($P < 0.025$).

Histopathologic Analysis

Of 40 donor eyes with a histopathologic diagnosis of neovascular AMD, 2 eyes (5.0%) exhibited an onion sign on ex vivo SD OCT imaging. Ex vivo SD OCT and histologic analysis for patient 1, a 98-year-old white woman, are shown in Figure 3. Figure 3A, C shows an approximately 1.2 × 0.66-mm dome-shaped RPE elevation with a hyperreflective surface and an outwardly convex base temporal to the foveal center. Figure 3A shows within the dome 3 groups of thin hyperreflective lines, radiating from a point on the temporal side, resembling a clinical onion sign. The histologic results in Figure 3B show that the dome has 3 groups of linear clefts at angles corresponding exactly to the hyperreflective bands, surrounded by hemorrhage (abundant erythrocytes without formed vascular endothelium) and overlying an outwardly convex Bruch's membrane. Six additional onion signs were visible by ex vivo SD OCT in this eye, including 2 more domes and 4 low, flat elevations. All corresponded to reflective plaques visible in red-free SLO (not shown). In a dense fibrovascular scar with both subretinal and sub-RPE components were several lucent slits consistent with cholesterol clefts (not shown)[11] that had not been apparent on prior ex vivo imaging.

Figure 3C shows the RPE elevation of patient 1 in a more inferiorly located B-scan, where it is associated with 3 hyperreflective foci within the neurosensory retina, each with distinct cellular content. Figure 3D shows intraretinal RPE cells, which are irregularly shaped and packed with black spindle-shaped melanosomes and green-staining lipofuscin granules. Figure 3E, F shows cells with lipid droplets stained tan, signifying lipid, and few (Fig 3E) or absent (Fig 3F) RPE granules. Relative to the intraretinal RPE in Figure 3D, these tan-staining cells are larger and more spherical, and they are clustered. We interpret cells in Figure 3E, F as phagocytes of monocytic origin that ingested and retained varying numbers of RPE granules while also differentiating into foam cells. Elsewhere in these sections are intraretinal fluid pockets and more hyperreflective foci (not shown).

Ex vivo multimodal imaging and histologic analysis for patient 2, a 91-year-old white man, are shown in Figures 4 and 5. Figure 4A is a color image showing a large, vertically elongated atrophic central area with punctate hyperpigmentation and ringed 270° by hyperpigmentation, representing an pigment epithelial detachment (PED). Within the central 0.7 mm, the PED is visible through the foveal floor as yellowish with punctate pigmentation, surrounded by golden hyperpigmentation with a sharp central border. Figure 4B shows that on 787-nm autofluorescence imaging, the PED is hypoautofluorescent with lobulated hyperautofluorescent borders. Figure 4C, D shows 2 ex vivo SD OCT scans through the PED, which measured 3.720 × 2.583 mm (superior-inferior × nasal-temporal). Intraretinal fluid pockets 1.38 and 0.69 mm in length were located temporal and nasal to the PED, respectively, and a 0.15-mm-long fluid pocket was present in the fovea (not shown). Increased light transmitted through the PED apex (Fig 4C, D) revealed numerous horizontal hyperreflective lines with scattered tiny hyperreflective spots against an inhomogeneous background reflectivity. One intense reflectivity source appeared as a thin line on SD OCT and a plaque on NIR SLO (not shown), suggesting a thin, flat shape. The RPE band on the PED dome was irregular, with small hyperreflective spots between RPE and photoreceptors. In 2 locations on the PED dome (0.150 and 0.300 mm in length), the RPE band was thicker and associated with hyperreflective spots within the overlying neurosensory retina.

The histologic analysis for patient 2 shows that the PED contains lucent linear clefts (Figs 4E and 5A, 1) cutting across several phases of fluid (Fig 5A, 2−4) that correspond to the hyperreflective lines and background reflectivity in SD OCT, respectively. The fluid phases contain lipid, indicated by tan staining, and contrast with clear plasma in choriocapillaries (Fig 5A, arrow, 2, and 3). Fluid from the PED and oily BLinD flanking the PED meet at a distinct phase boundary, emphasizing their different physical characteristics (Fig 5B, arrow). Judging from debris adhering to the PED undersurface (Fig 5B, arrowheads) and flocculent material within the PED (Fig 5A, 4), the fluid may arise from within BLinD and dislodge pieces of this material. Within the PED fluid, macrophages with irregularly shaped cell bodies and inclusions that are large, deep brown, polydisperse, and unevenly packed account for the hyperreflective spots (Fig 4E). Sloughed RPE cells together with small areas of RPE atrophy on the PED apex account for the irregular pigmentation and 787-nm autofluorescence pattern in the en face view (Fig 4A, B). Intraretinal cysts containing tan-staining fluid with lipid droplets and cells shown in Figure 4F−I together account for the intraretinal hyporeflective cavities and hyperreflective spots, respectively. The cells have evenly spaced spindle-shaped melanosomes and green-to-bronze-staining lipofuscin granules consistent with intraretinal RPE (Fig 4G, H) or polydisperse irregular inclusions consistent with phagocytes of monocytic origin (Fig 4F, I).

Discussion

To our knowledge, this study is the first to report frequency, natural history, and histologic correlates of the onion sign in neovascular AMD. A long-lasting yet dynamic structure, the onion sign was visible in approximately 5% to 7% of neovascular AMD eyes and associated positively with intraretinal or subretinal hyperreflective foci and intraretinal fluid. A possible association between the onion sign and systemic hypercholesterolemia was suggested by a significantly higher use of cholesterol-lowering medications in cases compared with controls. Histologic analysis of 2 patients with RPE elevation and sub-RPE hemorrhage or fluid revealed that hyperreflective lines correlated with clefts created by the extraction of cholesterol crystals during tissue processing (Supplemental Fig 2, available online at www.aaojournal.org). Such crystals were reported in human eye pathologic settings[11,19] and in experimental

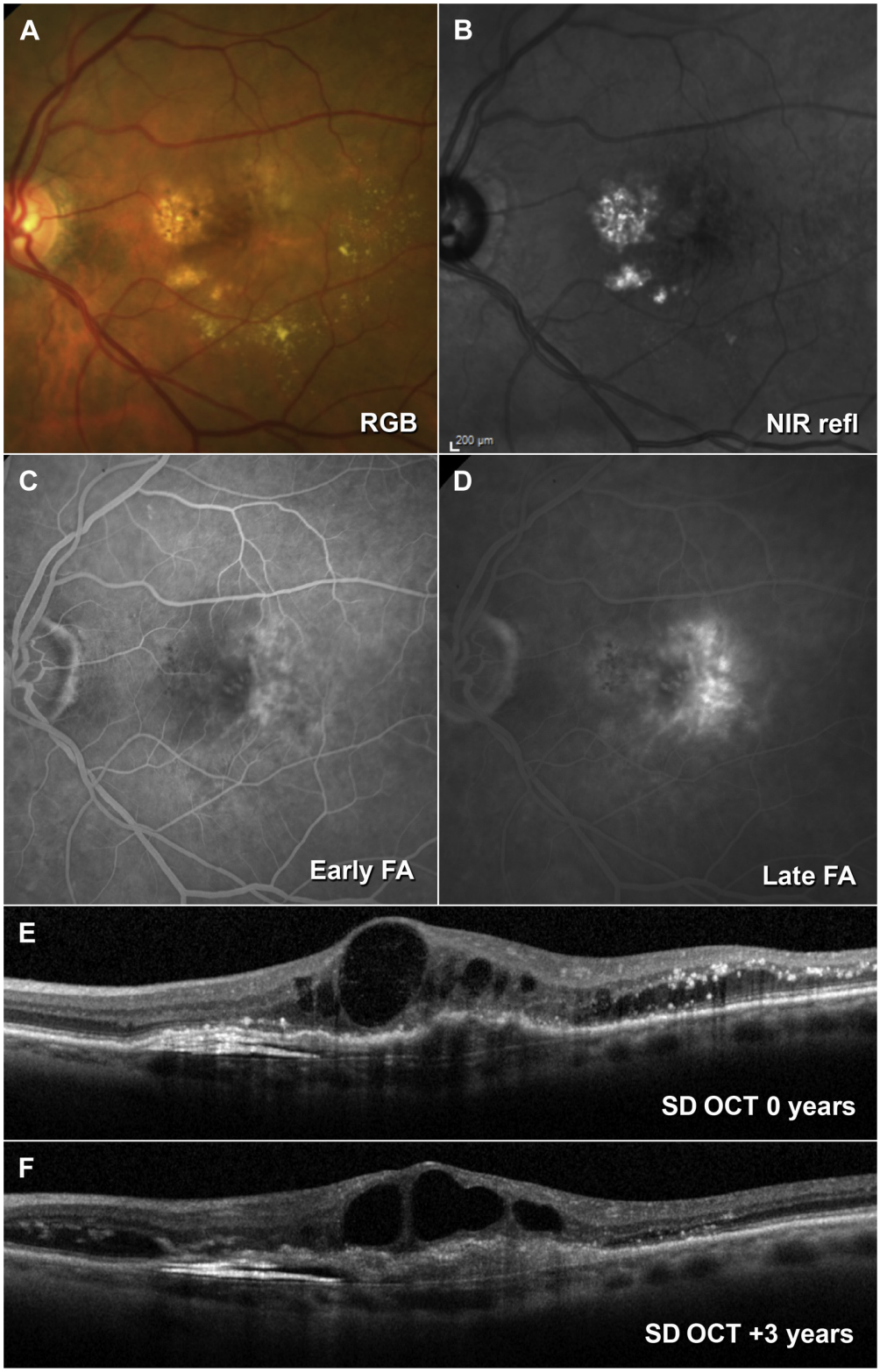

Figure 1. Multimodal imaging of the onion sign in neovascular age-related macular degeneration in a 72-year-old white woman with exudative changes. **A**, Color fundus photograph (RGB) showing yellow-gray exudation just nasal to the fovea and circinate yellow exudates. **B**, Near-infrared reflectance scanning laser ophthalmoscope (NIR-refl) image showing hyperreflectivity of the yellow-gray exudates nasal to the fovea. **C**, Early fluorescein angiogram (FA) showing hyperfluorescence temporal to the fovea consistent with neovascularization. **D**, Late FA showing late leakage, also consistent with neovascularization, but not colocalizing with the onion sign. **E**, Spectral-domain optical coherence tomography (SD OCT) scan through the fovea showing the onion sign nasal to the fovea, consisting of multiple layered hyperreflective lines below the retinal pigment epithelium. There are multiple intraretinal hyperreflective foci temporal to the fovea. **F**, Spectral-domain optical coherence tomography scan through the fovea 3 years later showing persistence of the onion sign, with fewer hyperreflective lines.

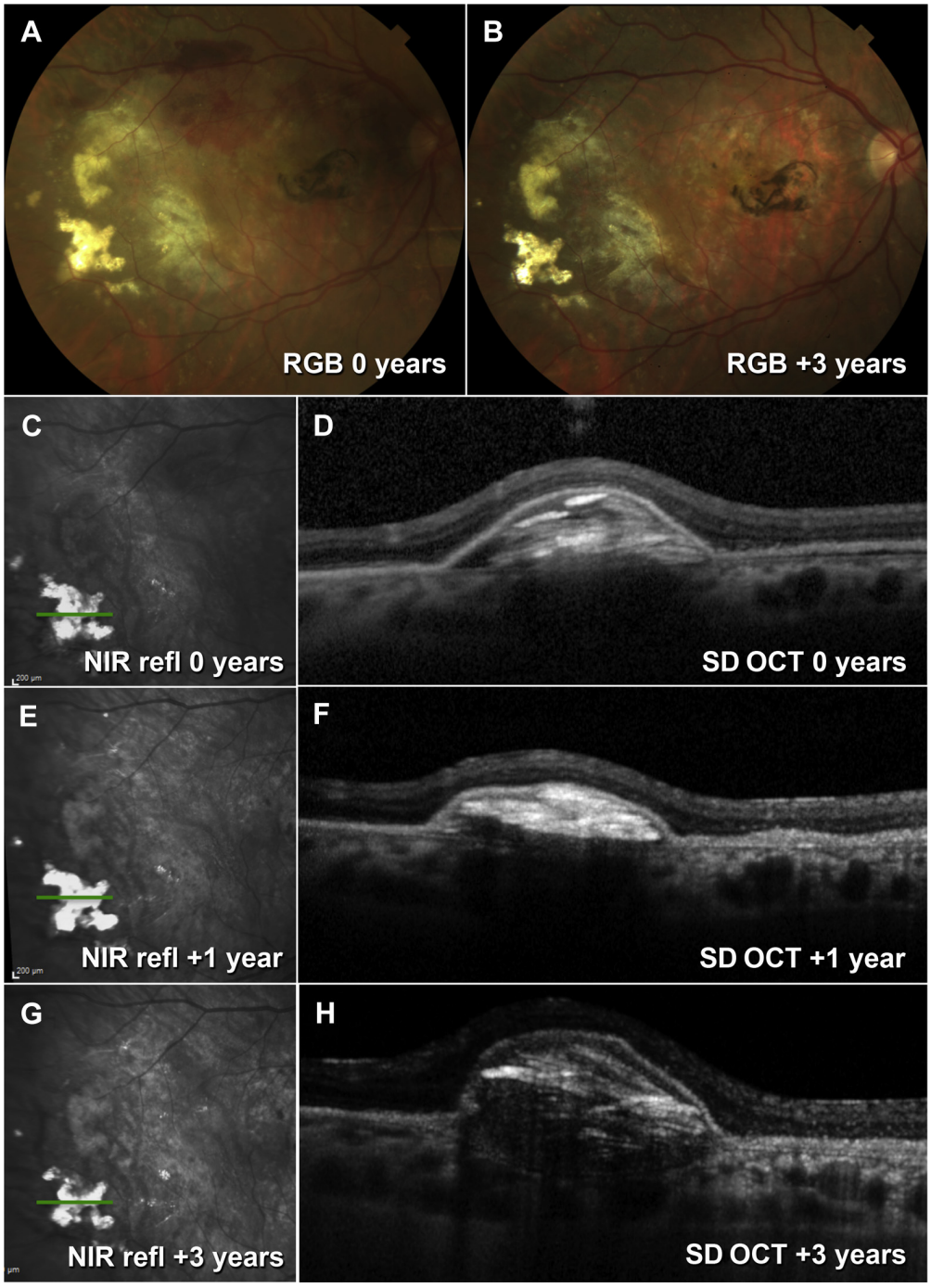

Figure 2. Images showing how the onion sign in neovascular age-related macular degeneration fluctuates in size and complexity in a 67-year-old white woman with exudative macular changes. **A**, Color fundus photograph (RGB) showing refractile yellow exudation temporal to the macula that occurred while the patient was receiving intravitreal ranibizumab injections. **B**, Color fundus photograph obtained 3 years later showing the same refractile yellow exudation. **C**, **D**, Near-infrared reflectance (NIR) scanning laser ophthalmoscope (SLO; NIR refl) and spectral-domain optical coherence tomography (SD OCT) images obtained at this visit showing that the hyperreflective lesion on NIR SLO corresponds to an onion sign consisting of multiple layered hyperreflective lines below the elevated retinal pigment epithelium. **E**, **F**, Corresponding NIR SLO and SD OCT images obtained 1 year later showing persistence of the onion sign, with reduced dome height and fewer clearly discernible hyperreflective lines. **G**, **H**, Corresponding NIR SLO and SD OCT images through the refractile exudates obtained 3 years later showing persistence of the onion sign, with increased dome height and more hyperreflective lines.

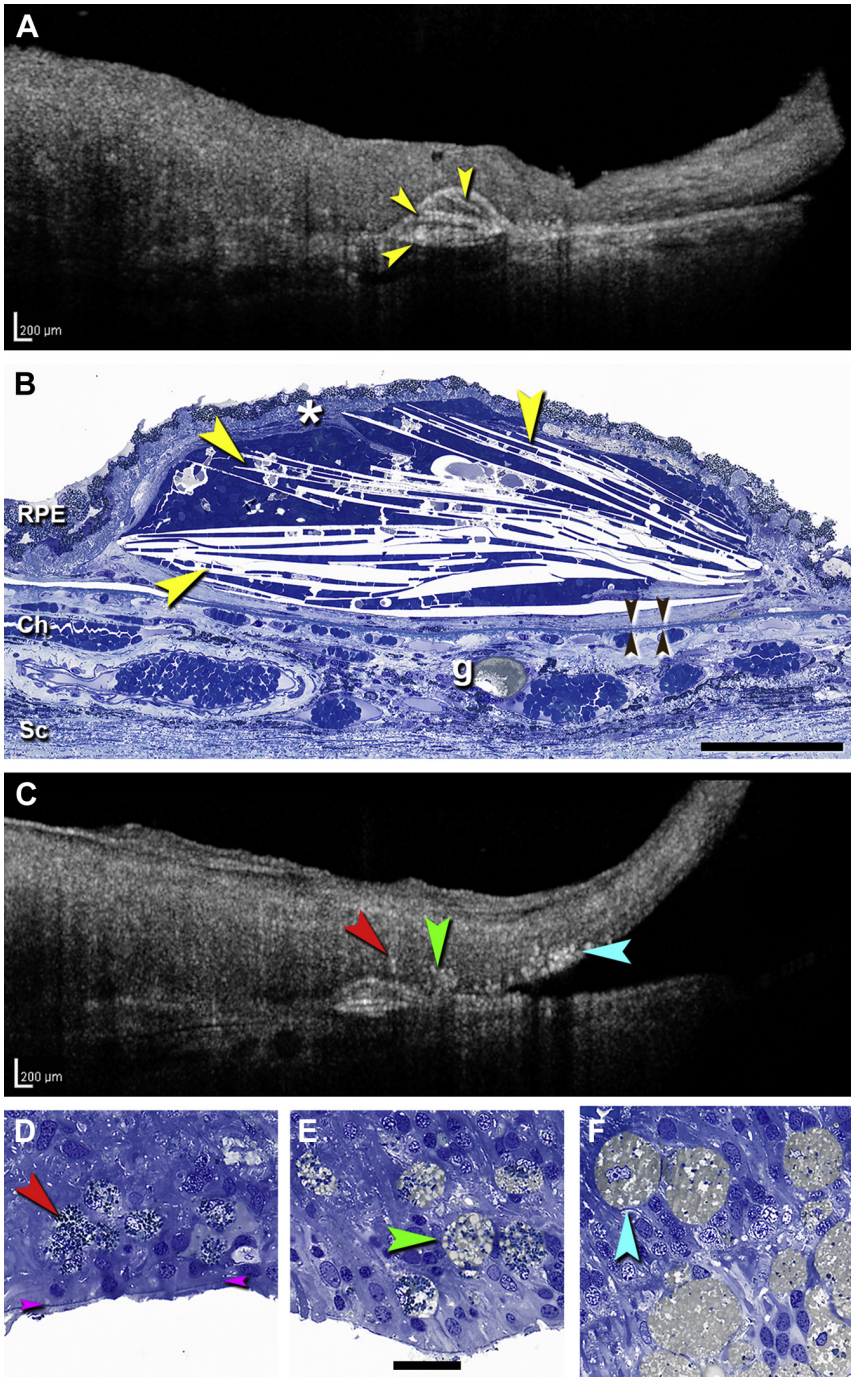

Figure 3. Ex vivo spectral-domain optical coherence tomography (SD OCT) image and photomicrographs showing histologic evidence of the onion sign in a submicrometer epoxy section from a 98-year-old white woman with neovascular age-related macular degeneration (stain, toluidine blue). **A**, Ex vivo SD OCT image showing 3 groups of thin highly hyperreflective lines (arrowheads) within an overall hyperreflective retinal pigment epithelium (RPE) elevation. The foveal center is nasal to the elevation (off the left edge). **B**, Histologic analysis revealing cholesterol clefts clustered in 3 planes corresponding to the hyperreflective lines in (**A**) (arrowheads). Bruch's membrane (black arrowheads) is bowed outward. *Basal laminar deposit; Ch = choroid; Sc = sclera; g = Friedman lipid globule.[61] Bar, 100 µm. **C**, Ex vivo SD OCT image through the same elevation at a location inferior to (**A**) showing 3 hyperreflective foci in the neurosensory retina that are magnified in (**D**) (red), (**E**) (green), and (**F**) (teal). Bar in (**E**), 25 µm, applies to (**D**–**F**). **D**, Intraretinal RPE has a full complement of black spindle-shaped melanosomes and green-staining lipofuscin granules. Cells of presumed monocytic origin with tan-staining lipid droplets and sparse (**E**) or absent (**F**) RPE melanosomes.

hypercholesterolemia,[20,21] where birefringence before processing and clefts after processing can be demonstrated directly (Supplemental material, available online at www.aaojournal.org). Our data thus support the original hypotheses that sub-RPE lipids are contributory[1] and that the contributing lipid has the chemical and physical form of crystalline cholesterol.[6]

We believe that the histologic cases from these clinically undocumented donors were neovascular AMD. Patient 1 had disciform degeneration in the setting of basal laminar deposit and BLinD. Patient 2 had a serous PED, intraretinal cysts, and hyperreflective spots in the same setting, yet a specific neovascular membrane was not found, likely because of the spacing of our standard section planes. For example, type 3 neovascularization is focal[22,23] and could have been missed. However, the combination of a PED and intraretinal fluid in patient 2 merited consideration as neovascular AMD. Although histologic analysis used eyes different from those imaged clinically, attribution of hyperreflective lines to cholesterol clefts is justified, as follows: highly similar appearance of ex vivo and in vivo hyperreflective lines, distinctive appearance of cholesterol clefts, the clinically observed transmissivity characteristics,[6] histologically validated imaging of crystals in cardiovascular disease, similar clinical and histologic prevalence in neovascular AMD eyes, and excellent preservation of donor eyes, reducing probability of artifact. Because donor tissues were recovered before 2006, it can be concluded that the onion sign is not a consequence of anti-VEGF therapy, although we cannot exclude an effect of other treatments unknown to us. Eyes not treated by anti-VEGF therapy may be more likely to progress quickly to scars. The onion sign may develop preferentially in eyes with chronic exudation with absence of rapid neovascularization growth or hemorrhage from type 1 neovascularization. Chronic treatment with anti-VEGF agents in eyes showing some resistance and persistent leakage may predispose to this finding. Thus, the similar frequency in a clinic population and treatment-naïve donors was somewhat surprising. Although we have not observed onion signs in non-neovascular AMD eyes in our clinical practice, others have[4] (Supplementary material, available online at www.aaojournal.org), making it premature to conclude that this sign localizes exclusively to neovascular disease. It is plausible that onion signs occur in serous PEDs and subclinical focal neovascularization indistinguishable by fluorescein or indocyanine green angiography. We restricted our current investigations to neovascular AMD.

Cholesterol crystal formation is important for atherosclerotic cardiovascular disease, forming early, instigating inflammation, and contributing to sudden cardiac events.[24] Optical coherence tomography imaging of coronary artery plaques yields curvilinear hyperreflective lines corresponding to histologically confirmed crystals.[7] Cholesterol has 2 chemical forms, unesterified cholesterol (UC) and esterified cholesterol (EC; bound to a fatty acid). It also has 3 physical forms that vary in proportions of UC, EC, and solubilizing phospholipid: droplets (EC, UC, phospholipid); membranes (UC, phospholipid); and crystals (UC only).[25] Crystal formation in supersaturated solutions is affected by local physical factors, with cooler temperatures, lower pH, and higher saturation promoting formation[26] and degree of hydration affecting crystal shape (monohydrate, rhomboid plates; anhydrous, aciculate, or needle-shaped).[27] Our data suggest that appreciable lipid content in fluid (patient 2) and red blood cells (patient 1)[28] is a potential contributor to UC supersaturation.[24,29]

It seems that supersaturation and subsequent crystal formation in PED requires an aqueous microenvironment that is distinct from the oily microenvironment of soft drusen and BLinD[30] (Fig 5). Drusen are extracellular lesions in the sub-RPE compartment that provide a cleavage plane for invading neovessels.[31] The largest volumetric component of drusen is lipid, especially EC, UC, and phosphatidylcholine, attributed to RPE-secreted lipoprotein particles containing apolipoproteins B and E in a pathway driven by dietary lipid recycling in the outer retina.[32] Evidence for this model includes accumulation in Bruch's membrane throughout adulthood of solid particles with classic lipoprotein morphologic features containing cholesteryl esters rich in linoleate, RPE expression of hallmark lipoprotein secretion genes, secretion of apolipoprotein E-immunoreactive lipoprotein-like particles by highly differentiated cultured RPE, and the inconsistent association of AMD at the person level with plasma lipoprotein levels.[33] Another cholesterol source contributing to sub-RPE supersaturation is lipoproteins of systemic origin. The absence of cholesterol crystals from Bruch's membrane and drusen has been thought to be a crucial difference between AMD and systemic atherosclerosis, 2 diseases unified by early lipoprotein deposition in vessel walls.[34] Thus, we propose that crystals represented by the onion sign have an important systemic contribution via plasma exudates, supported by the association with self-reported cholesterol-lowering medication. Although this retrospective study was limited by the lack of serum cholesterol data, this initial association between the onion sign and self-reported use of oral cholesterol-lowering medication can encourage future studies to investigate this relationship in detail. If our clinical findings are replicated, it may be possible that onion signs in AMD patients signify systemic hypercholesterolemia that should be monitored.

Sub-RPE cholesterol crystallization joins etiologically diverse retinal disorders with crystals, including Bietti crystalline dystrophy (*CYP4V2* mutations),[19,35] cerebrotendinous xanthomatosis (*CYP27A1* mutations),[36] intraretinal crystals in macular telangiectasia type 2[37] and in AMD,[2] preretinal crystals associated with triamcinolone usage,[38] and refractile hydroxyapatite spherules in calcifying drusen.[39,40] The onion sign also is distinct from other sub-RPE hyperreflective material such as fibrovascular scars, with horizontal reflectivities caused by densely packed planes of collagen and fibroblasts. Other SD OCT features with potential as crystalline are so-called plaques, single hyperreflective horizontal lines parallel to and very close to Bruch's membrane, described by Fleckenstein et al[41] and used as progression markers.[42] Yet cholesterol crystals in this location have not been illustrated by major

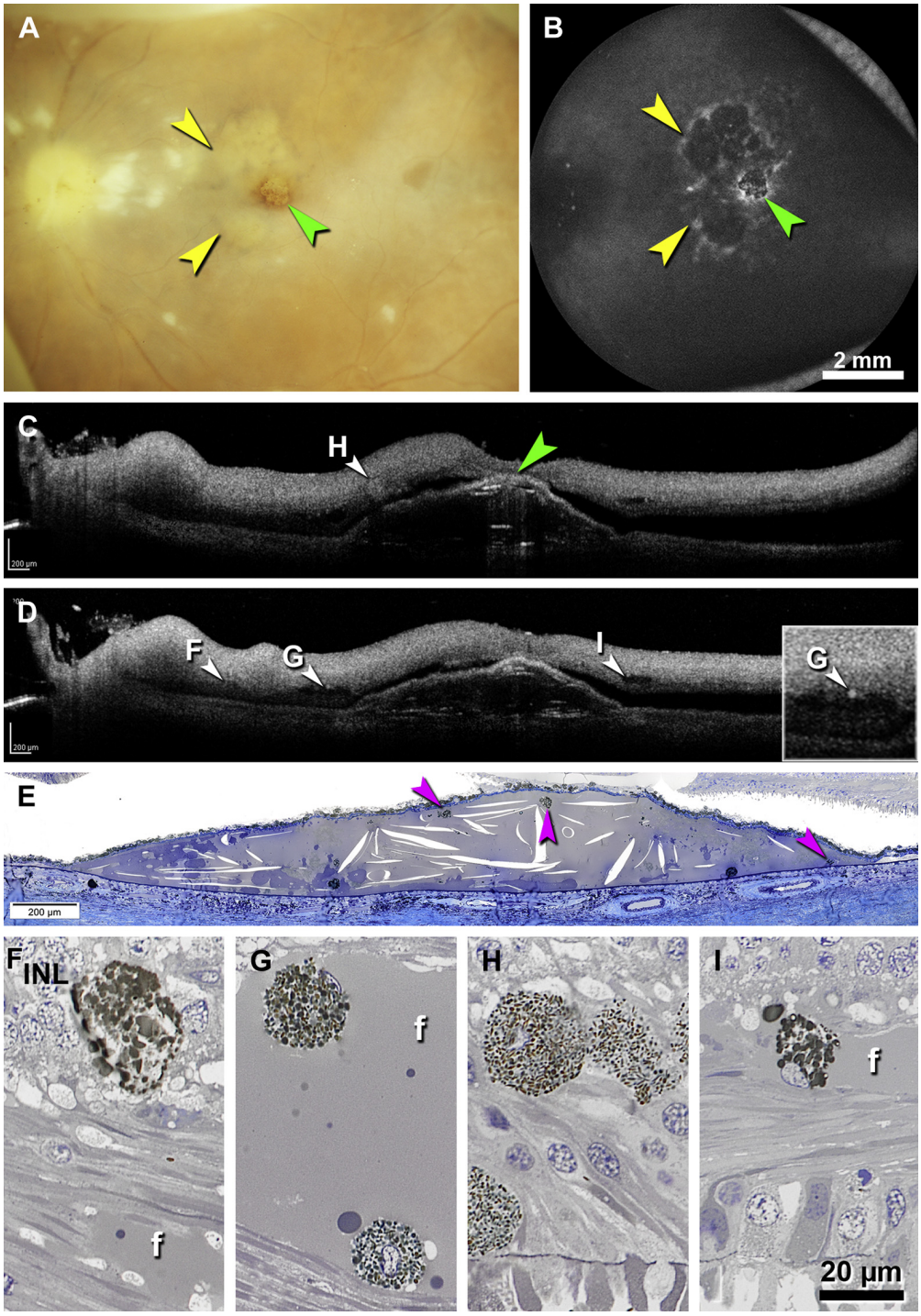

Figure 4. Ex vivo imaging and histologic analysis of a pigment epithelial detachment (PED) with an onion sign and associated hyperreflective foci in a submicrometer epoxy section from a 91-year-old white man with neovascular age-related macular degeneration (stain, toluidine blue). **A**, Color photography showing retinal pigment epithelium detachment (PED, yellow) that is prominent at the fovea (green). Cotton wool spots (white clumps between the PED and the optic nerve head) are visible in color and near-infrared reflectance scanning laser ophthalmoscopy (not shown); they are not visible in 787-nm autofluorescence (**B**). **B**, Autofluorescence at 787 nm showing that the PED (green) is hypoautofluorescent with a hyperautofluorescent border (yellow). **C**, **D**, Spectral-domain optical coherence tomography scans (**C**) through and (**D**) inferior to the foveal center showing horizontal hyperreflective lines within the PED (green). Median length of clefts is 105.1 µm (range, 39.9–533.9 µm). Hyperreflective foci are in (**F**–**I**). **D**, (insert **G**) was brightened to highlight a hyperreflective spot believed to represent one or several cells. **E**, Histologic processing resulting in the extraction of numerous lucent needle-shaped clefts in the PED that are cholesterol crystals. Cells in the fluid (pink) are presumed macrophages. **F**–**I**, Photomicrographs showing presumed macrophages with polydisperse irregular inclusions. Intraretinal RPE has spindle-shaped melanosomes and monodisperse green-stained lipofuscin. Original magnification, panels **E**–**I**, 60X. f = fluid.

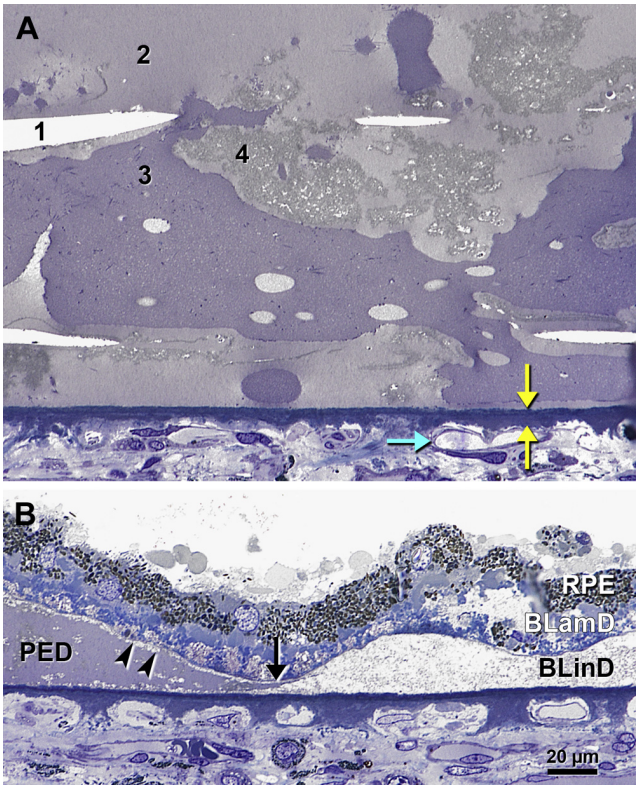

Figure 5. Photomicrographs showing the contents and microenvironment of a large pigment epithelial detachment (PED) with an onion sign in the same eye as Figure 4. **A**, Cholesterol clefts (1), and 3 fluid phases containing lipid (2–4; 4 denotes flocculent material apparently originating from lipoprotein-derived debris in adjoining basal linear deposit [BLinD]). Teal arrow, choriocapillary with clear plasma; yellow arrows, Bruch's membrane. **B**, At the margin of the onion sign–bearing PED, fluid meets oily BLinD at a phase boundary (black arrow). Debris adheres to the PED undersurface (black arrowheads). BLamD = basal laminar deposit; RPE = retinal pigment epithelium. Bar, 20 μm.

AMD histologic surveys.[12,43–47] Whether these plaques are onion sign precursors thus awaits further information.

Beyond showing cholesterol clefts, the histologic cases provided unexpected insight into RPE fate over localized elevations of 2 different compositions (hemorrhage and fluid). For the first time, hyperreflective foci associated with intraretinal fluid in ex vivo SD OCT were tracked to specific individual cells. Hyperreflective foci found in all 16 clinical cases now also are plausibly attributable to such cells. Recently, we extensively surveyed RPE morphologic features in advanced AMD, also using high-resolution histologic analysis, to disclose characteristic RPE organelles and basal laminar deposit.[17] Two cellular phenotypes with a full complement of RPE granules that apparently form an anterior migratory pathway[17] also were present in our 2 patients. Many authors consider these cells to be macrophages or microglia.[48–51] In patient 1, some cells conferring hyperreflectivity are more readily attributable to cells of monocytic origin than to phagocytized RPE. These monocyte-derived cells retained telltale melanosomes, while also engorging with lipid droplets like foam cells. Foam cells are hyperreflective in coronary artery plaques.[7] Because we have not seen a resident population of nonpigmented cells in the subretinal space[52] of human donor eyes, we suggest that the lipid-filled cells are microglia that moved from inner to outer retina, because they do in degenerations and injuries.[53] Intriguingly, mouse microglia in vitro can take up 7-ketocholesterol, a proinflammatory oxysterol found in aging Bruch's membrane and drusen,[54] and form intracellular lipid droplets.[55] It is tempting to speculate that microglia constitute 1 population of hyperreflective spots and that anteriorly migrating RPE constitutes another. One way to test this hypothesis is to determine whether cells are separable by size, clumping, motility, and characteristics in multimodal imaging studies.[49,56]

Although identifying the histologic features of a clinically characterized eye is considered a gold standard, our study notably identified a correlate to an in vivo SD OCT imaging sign in an ex vivo SD OCT screen of archived donor eyes. Limitations of this study include the absence of crystal quantification in clinical and histologic PED and molecular phenotyping of intraretinal hyperreflective cells. Nevertheless, data support the concept that SD OCT is an essential tool for characterizing donor eyes in the pathology laboratory.[57–59] Targeting single cells of known reflectivity characteristics for labeling studies will be a powerful means of linking molecular discovery with contemporary clinical imaging. This capability is important because the combination of comprehensive anatomic pathologic features and excellent clinical imaging is treasured in ophthalmology yet still a rarity,[60] and laboratory animals lacking a macula do not yet faithfully replicate AMD.

Acknowledgments. The authors thank the personnel of the Alabama Eye Bank (Doyce V. Williams, Executive Director, and Alan S. Blake, Chief Technical Officer) for timely retrieval of donor eyes and Giovanni Staurenghi, MD, for facilitating the participation of Dr. Zanzottera.

References

1. Mukkamala SK, Costa RA, Fung A, et al. Optical coherence tomographic imaging of sub-retinal pigment epithelium lipid. Arch Ophthalmol 2012;130:1–7.
2. Lima LH, Freund KB, Klancnik JM Jr, Spaide RF. Intraretinal crystalline deposits in neovascular age-related macular degeneration. Retina 2010;30:542–7.
3. Coscas G. Optical Coherence Tomography in Age-Related Macular Degeneration. Berlin: Springer; 2009.
4. Querques G, Georges A, Ben Moussa N, et al. Appearance of regressing drusen on optical coherence tomography in age-related macular degeneration. Ophthalmology 2014;121:173–9.
5. Bonnet C, Querques G, Zerbib J, et al. Hyperreflective pyramidal structures on optical coherence tomography in geographic atrophy areas. Retina 2014;34:1524–30.
6. Christakopoulos C, Pryds A, Larsen M. Subretinal lamellar bodies in polypoidal choroidal vasculopathy. Acta Ophthalmol 2013;91:e248–9.
7. Liu L, Gardecki JA, Nadkarni SK, et al. Imaging the subcellular structure of human coronary atherosclerosis using micro-optical coherence tomography. Nat Med 2011;17:1010–4.

8. Tearney GJ, Jang IK, Bouma BE. Optical coherence tomography for imaging the vulnerable plaque. J Biomed Opt 2006;11:021002.
9. Yonetsu T, Bouma BE, Kato K, et al. Optical coherence tomography: 15 years in cardiology. Circ J 2013;77:1933–40.
10. Abela GS, Aziz K. Cholesterol crystals rupture biological membranes and human plaques during acute cardiovascular events—a novel insight into plaque rupture by scanning electron microscopy. Scanning 2006;28:1–10.
11. Green WR, Key SN 3rd. Senile macular degeneration: a histopathologic study. Trans Am Ophthalmol Soc 1977;75: 180–254.
12. Curcio CA, Presley JB, Millican CL, Medeiros NE. Basal deposits and drusen in eyes with age-related maculopathy: evidence for solid lipid particles. Exp Eye Res 2005;80:761–75.
13. Litts KM, Messinger JD, Dellatorre K, et al. Clinicopathological correlation of outer retinal tubulation in age-related macular degeneration. JAMA Ophthalmol 2015;133:609–12.
14. Curcio CA, Messinger JD, Mitra AM, et al. Human chorioretinal layer thicknesses measured using macula-wide high resolution histological sections. Invest Ophthalmol Vis Sci 2011;52:3943–54.
15. Curcio CA, Medeiros NE, Millican CL. The Alabama Age-Related Macular Degeneration Grading System for donor eyes. Invest Ophthalmol Vis Sci 1998;39:1085–96.
16. Staurenghi G, Sadda S, Chakravarthy U, Spaide RF. Proposed lexicon for anatomic landmarks in normal posterior segment spectral-domain optical coherence tomography: The IN*OCT Consensus. Ophthalmology 2014;121:1572–8.
17. Zanzottera EC, Messinger JD, Ach T, et al. The Project MACULA retinal pigment epithelium grading system for histology and optical coherence tomography in age-related macular degeneration. Invest Ophthalmol Vis Sci 2015;56: 3253–68.
18. Ford ES, Li C, Pearson WS, et al. Trends in hypercholesterolemia, treatment and control among United States adults. Int J Cardiol 2010;140:226–35.
19. Wilson DJ, Weleber RG, Klein ML, et al. Bietti's crystalline dystrophy. A clinicopathologic correlative study. Arch Ophthalmol 1989;107:213–21.
20. Ramírez AI, Salazar JJ, De Hoz R, et al. Macroglial and retinal changes in hypercholesterolemic rabbits after normalization of cholesterol levels. Exp Eye Res 2006;83:1423–38.
21. Salazar JJ, Ramírez AI, de Hoz R, et al. Alterations in the choroid in hypercholesterolemic rabbits: reversibility after normalization of cholesterol levels. Exp Eye Res 2006;84:412–22.
22. Monson DM, Smith JR, Klein ML, Wilson DJ. Clinicopathologic correlation of retinal angiomatous proliferation. Arch Ophthalmol 2008;126:1664–8.
23. Nagiel A, Sarraf D, Sadda SR, et al. Type 3 neovascularization: evolution, association with pigment epithelial detachment, and treatment response as revealed by spectral domain optical coherence tomography. Retina 2015;35:638–47.
24. Abela GS. Cholesterol crystals piercing the arterial plaque and intima trigger local and systemic inflammation. J Clin Lipidol 2010;4:156–64.
25. Small DM. George Lyman Duff Memorial Lecture. Progression and regression of atherosclerotic lesions. Insights from lipid physical biochemistry. Arteriosclerosis 1988;8: 103–29.
26. Vedre A, Pathak DR, Crimp M, et al. Physical factors that trigger cholesterol crystallization leading to plaque rupture. Atherosclerosis 2009;203:89–96.
27. Uskokovic V. Insights into morphological nature of precipitation of cholesterol. Steroids 2008;73:356–69.
28. Virmani R, Kolodgie FD, Burke AP, et al. Atherosclerotic plaque progression and vulnerability to rupture: angiogenesis as a source of intraplaque hemorrhage. Arterioscler Thromb Vasc Biol 2005;25:2054–61.
29. Duewell P, Kono H, Rayner KJ, et al. NLRP3 inflammasomes are required for atherogenesis and activated by cholesterol crystals. Nature 2010;464:1357–61.
30. Curcio CA, Johnson M, Huang J-D, Rudolf M. Aging, age-related macular degeneration, and the response-to-Retention of apolipoprotein B-containing lipoproteins. Prog Ret Eye Res 2009;28:393–422.
31. Killingsworth MC, Sarks JP, Sarks SH. Macrophages related to Bruch's membrane in age-related macular degeneration. Eye 1990;4:613–21.
32. Curcio CA, Johnson M, Rudolf M, Huang J-D. The oil spill in ageing Bruch's membrane. Br J Ophthalmol 2011;95: 1638–45.
33. Pikuleva I, Curcio CA. Cholesterol in the retina: the best is yet to come. Prog Ret Eye Res 2014;41:64–89.
34. Curcio CA, Johnson M, Huang J-D, Rudolf M. Apolipoprotein B-containing lipoproteins in retinal aging and age-related maculopathy. J Lipid Res 2010;51:451–67.
35. Pennesi ME, Weleber RG. High-resolution optical coherence tomography shows new aspects of Bietti crystalline retinopathy. Retina 2010;30:531–2.
36. Dotti MT, Rufa A, Federico A. Cerebrotendinous xanthomatosis: heterogeneity of clinical phenotype with evidence of previously undescribed ophthalmological findings. J Inherit Metab Dis 2001;24:696–706.
37. Sallo FB, Leung I, Chung M, et al. Retinal crystals in type 2 idiopathic macular telangiectasia. Ophthalmology 2011;118: 2461–7.
38. Sarraf D, Vyas N, Jain A, et al. Triamcinolone-associated crystalline maculopathy. Arch Ophthalmol 2010;128:685–90.
39. Suzuki M, Curcio CA, Mullins RF, Spaide RF. Refractile drusen: clinical imaging and candidate histology. Retina 2015;35:859–65.
40. Thompson RB, Reffatto V, Bundy JG, et al. Identification of hydroxyapatite spherules provides new insight into subretinal pigment epithelial deposit formation in the aging eye. Proc Natl Acad Sci U S A 2015;112:1565–70.
41. Fleckenstein M, Charbel Issa P, Helb HM, et al. High-resolution spectral domain-OCT imaging in geographic atrophy associated with age-related macular degeneration. Invest Ophthalmol Vis Sci 2008;49:4137–44.
42. Moussa K, Lee JY, Stinnett SS, Jaffe GJ. Spectral domain optical coherence tomography-determined morphologic predictors of age-related macular degeneration-associated geographic atrophy progression. Retina 2013;33:1590–9.
43. Sarks SH. Ageing and degeneration in the macular region: a clinico-pathological study. Br J Ophthalmol 1976;60:324–41.
44. van der Schaft TL, Mooy CM, de Bruijn WC, et al. Histologic features of the early stages of age-related macular degeneration. Ophthalmology 1992;99:278–86.
45. Green WR, Enger C. Age-related macular degeneration histopathologic studies: the 1992 Lorenz E. Zimmerman Lecture. Ophthalmology 1993;100:1519–35.
46. Sarks S, Cherepanoff S, Killingsworth M, Sarks J. Relationship of basal laminar deposit and membranous debris to the clinical presentation of early age-related macular degeneration. Invest Ophthalmol Vis Sci 2007;48:968–77.
47. Curcio CA, Messinger JD, Sloan KR, et al. Subretinal drusenoid deposits in non-neovascular age-related macular degeneration: morphology, prevalence, topography, and biogenesis model. Retina 2013;33:265–76.

48. Buschini E, Piras A, Nuzzi R, Vercelli A. Age related macular degeneration and drusen: neuroinflammation in the retina. Prog Neurobiol 2011;95:14–25.
49. Gocho K, Sarda V, Falah S, et al. Adaptive optics imaging of geographic atrophy. Invest Ophthalmol Vis Sci 2013;54:3673–80.
50. Leuschen JN, Schuman SG, Winter KP, et al. Spectral-domain optical coherence tomography characteristics of intermediate age-related macular degeneration. Ophthalmology 2013;120:140–50.
51. Coscas G, De Benedetto U, Coscas F, et al. Hyperreflective dots: a new spectral-domain optical coherence tomography entity for follow-up and prognosis in exudative age-related macular degeneration. Ophthalmologica 2013;229:32–7.
52. Xu H, Chen M, Manivannan A, et al. Age-dependent accumulation of lipofuscin in perivascular and subretinal microglia in experimental mice. Aging Cell 2008;7:58–68.
53. Karlstetter M, Scholz R, Rutar M, et al. Retinal microglia: just bystander or target for therapy? Prog Retin Eye Res 2015;45:30–57.
54. Rodriguez IR, Clark ME, Lee JW, Curcio CA. 7-ketocholesterol accumulates in ocular tissues as a consequence of aging and is present in high levels in drusen. Exp Eye Res 2014;128:151–5.
55. Indaram M, Ma W, Zhao L, et al. 7-ketocholesterol increases retinal microglial migration, activation, and angiogenicity: a potential pathogenic mechanism underlying age-related macular degeneration. Sci Rep 2015;5:9144.
56. Lammer J, Bolz M, Baumann B, et al. Detection and analysis of hard exudates by polarization-sensitive optical coherence tomography in patients with diabetic maculopathy. Invest Ophthalmol Vis Sci 2014;55:1564–71.
57. Ghazi NG, Dibernardo C, Ying H, et al. Optical coherence tomography of peripheral retinal lesions in enucleated human eye specimens with histologic correlation. Am J Ophthalmol 2006;141:740–2.
58. Brown NH, Koreishi AF, McCall M, et al. Developing SDOCT to assess donor human eyes prior to tissue sectioning for research. Graefes Arch Clin Exp Ophthalmol 2009;247:1069–80.
59. Bagheri N, Bell BA, Bonilha VL, Hollyfield JG. Imaging human postmortem eyes with SLO and OCT. Adv Exp Med Biol 2012;723:479–88.
60. Klein ML, Wilson DJ. Clinicopathologic correlation of choroidal and retinal neovascular lesions in age-related macular degeneration. Am J Ophthalmol 2011;151:161–9.
61. Friedman E, Smith TR. Clinical and pathological study of choroidal lipid globules. Arch Ophthalmol 1966;75:334–6.

Footnotes and Financial Disclosures

Originally received: May 17, 2015.
Final revision: July 6, 2015.
Accepted: July 7, 2015.
Available online: August 19, 2015. Manuscript no. 2015-797.

[1] Vitreous Retina Macula Consultants of New York, New York, New York.
[2] LuEsther T. Mertz Retinal Research Center, Manhattan Eye, Ear, and Throat Institute, New York, New York.
[3] Department of Ophthalmology, University of Alabama School of Medicine, Birmingham, Alabama.
[4] Eye Clinic, Department of Clinical Science "Luigi Sacco," Sacco Hospital, University of Milan, Milan, Italy.
[5] Department of Ophthalmology, New York University School of Medicine, New York, New York.

Presented at: Association for Research in Vision and Ophthalmology Annual Meeting, 2015, Denver, Colorado.

Financial Disclosure(s):
The author(s) have made the following disclosure(s):
K.B.F.: Consultant - Genentech; Optos; Heidelberg Engineering; Thrombogenics; Optovue

Supported by the Macula Foundation (New York, NY); the LuEsther T. Mertz Retinal Research Center (New York, NY); the National Institutes of Health (NIH), Bethesda, Maryland (grant no.: R01 EY06109), and the National Eye Institute, NIH (grant no.: P30 EY003039); Research to Prevent Blindness, Inc., New York, New York; EyeSight Foundation of Alabama (Birmingham AL); the International Retinal Research Foundation (Birmingham AL); and the Arnold and Mabel Beckman Initiative for Macular Research (Irvine CA). Project MACULA received additional support from the Edward N. and Della L. Thome Memorial Foundation (Boston MA), and the International Retinal Research Foundation (Birmingham AL). The funding organizations had no role in the design and conduct of this study.

Author Contributions:

Conception and design: Pang, Messinger, Freund, Curcio

Analysis and interpretation: Pang, Messinger, Zanzottera, Curcio

Data collection: Pang, Messinger, Zanzottera, Curcio

Obtained funding: Curcio

Overall responsibility: Pang, Freund, Curcio

Abbreviations and Acronyms:
AMD = age-related macular degeneration; **BLinD** = basal linear deposit; **EC** = esterified cholesterol; **NIR** = near-infrared reflectance; **OCT** = optical coherence tomography; **PED** = pigment epithelial detachment; **RPE** = retinal pigment epithelium; **SD** = spectral-domain; **SLO** = scanning laser ophthalmoscopy; **UC** = unesterified cholesterol; **VEGF** = vascular endothelial growth factor.

Correspondence:
Christine A. Curcio, PhD, Department of Ophthalmology, EyeSight Foundation of Alabama Vision Research Laboratories, 1670 University Boulevard, Room 360, University of Alabama School of Medicine, Birmingham, AL 35294-0099. E-mail: curcio@uab.edu.

Supplementary material for

Pang C, Messinger JD, Zanzottera EC, Freund KB, Curcio CA. The Onion Sign in neovascular age-related macular degeneration corresponds to cholesterol crystals.

Table: Previous descriptions and illustrations consistent with the Onion Sign

First Author	Year	Reference	Authors' description	Patient population
Coscas	2009	[1]	Hyperreflective band	Neovascular AMD
Helb	2010	[2]	Well-defined strands of material with increased reflectivity	PED, neovascular AMD
Mukkamala	2012	[3]	Sub-RPE hyperreflective bands; Onion Sign; attributed to lipid	Neovascular AMD
Christakopoulos	2013	[4]	Subretinal lamellar bodies, attributed to cholesterol crystals	PED, polypoidal choroidal vasculopathy
Clemens	2013	[5]	Highly reflective, multilayered, laminar structures, usually orientated parallel to Bruch's membrane	PED, AMD
Garcia Filho	2013	[6]	Not described	Fibrovascular PED
Mrejen	2013	[7]	Sub-RPE hyperreflective bands; Onion Sign; attributed to lipid	Vascularized PED
Inoue	2014	[8]	Sub–RPE linear structures	Anti-VEGF treated neovascular AMD
Querques	2014	[9]	Multilaminar hyperreflective signal beneath RPE; attributed to Bruch's membrane	Non-exudative AMD

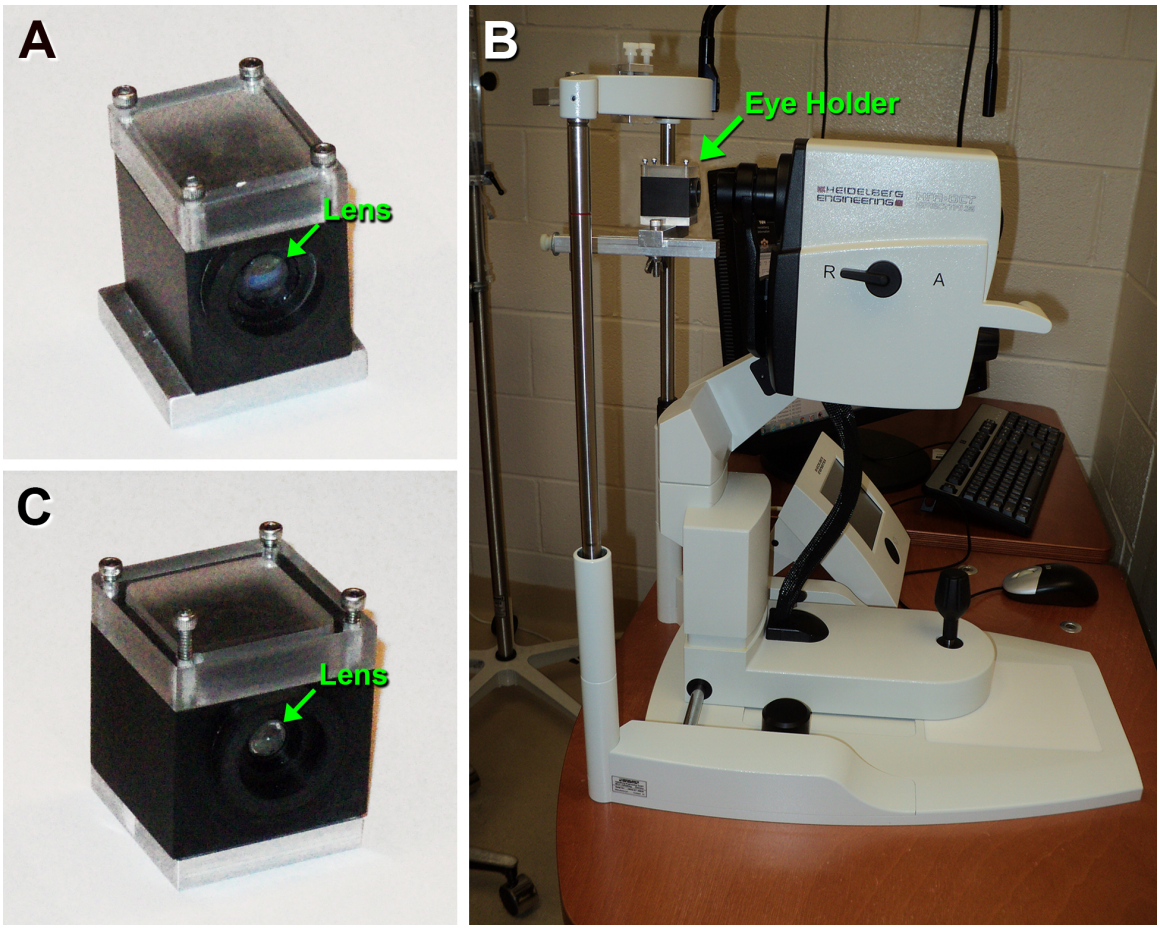

Supplementary Figure 1: Tissue holder for *ex vivo* imaging of donor eyes using the Spectralis. Original design was generated by J. Fischer (Heidelberg Engineering) and modified by author JDM. **A.** A fluid-filled chamber has a lid, tissue plate, and a 60D lens. Originally designed for optic nerve head studies [10], this device was used to hold 8.25 mm diameter full thickness macular punch, originally by sutures but more conveniently by pressure-fit. **B.** A large chamber can accommodate a human donor eye with the anterior segment removed and was used for eye-tracked SDOCT imaging in a direct clinicopathologic correlation [11]. **C.** Held in front of the Spectralis, the tissue in the chamber looks out of the lens into the optical path of the instrument.

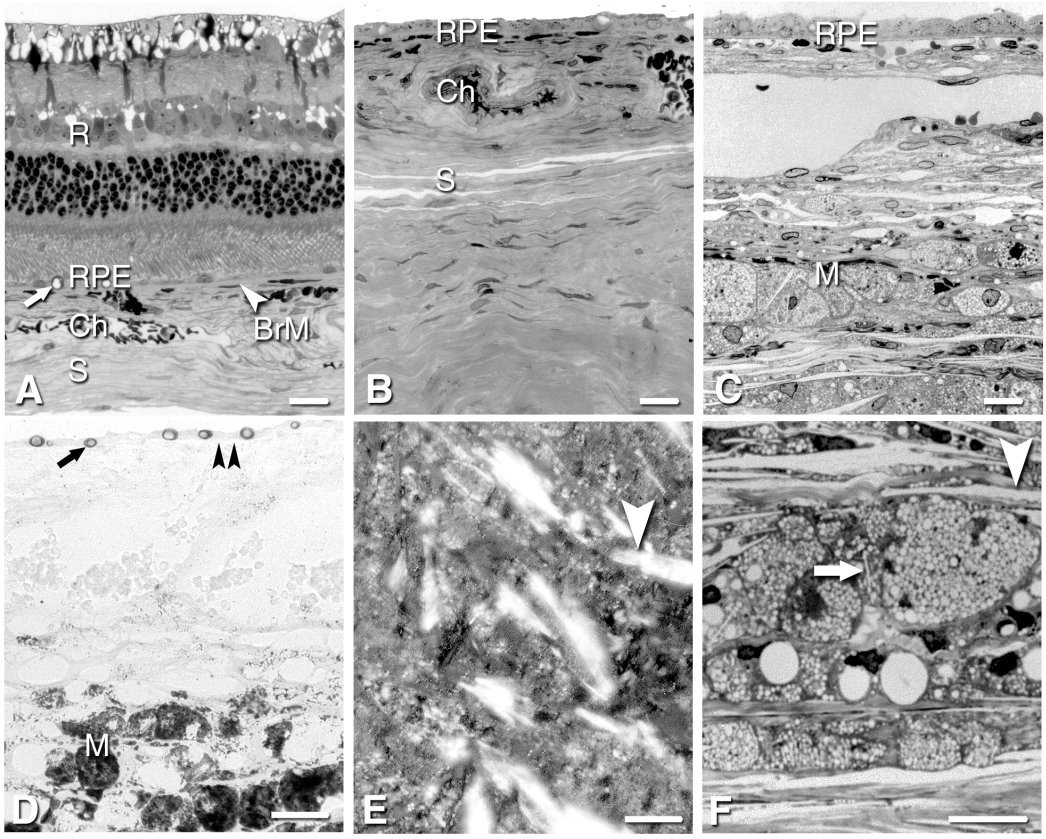

Supplementary Figure 2: Cholesterol crystals before and after extraction in experimental hypercholesterolemia. Rabbits consuming atherogenic diets [12, 13] for 3 months (C), 4 months (E,F), and 6 months (D) were compared to animals consuming control diets (A,B). **A.** Normal rabbit retina (R) retinal pigment epithelium (RPE), choroid (Ch), and sclera (S). Arrowhead, Bruch's membrane (BrM). Bar = 20 μm. **B.** Normal RPE and choroid lacks lipid accumulation. Bar = 20 μm. **C.** In a hypercholesterolemic rabbit, numerous lipid-filled macrophages infiltrate the suprachoroidal space [14, 15]. Bar = 20 μm. **D.** Macrophages (M) and RPE lipid droplets (arrow) contain oil red O binding lipids but BrM does not (black arrowheads) in a hypercholesterolemic rabbit; bar = 50 μm. **E.** Cholesterol crystals (white arrowheads) in the macrophage layer are refractile by polarizing microscopy. Bar = 50 μm. **F.** Histology-related extraction of cholesterol crystals leaves distinctive clefts outside (arrowhead) and inside (arrow) macrophages, 1 μm thick section, toluidine blue; bar = 20 μm. The atherogenic diets markedly raised total plasma cholesterol, with the greatest

increases in VLDL and LDL fractions and causing grossly visible aortic plaques, fatty liver, and cholesterol deposition in the cornea and ciliary processes [12]. Data were first presented at 2002 annual meeting of the Association for Research in Vision and Ophthalmology. [16] Study was approved by the Institutional Animal Care and Use Committee at UAB.

Literature Cited

1. Coscas G. Optical Coherence Tomography in Age-Related Macular Degeneration: Springer, 2009.
2. Helb HM, Charbel Issa P, Fleckenstein M, et al. Clinical evaluation of simultaneous confocal scanning laser ophthalmoscopy imaging combined with high-resolution, spectral-domain optical coherence tomography. Acta Ophthalmol 2010;88:842-9. PMID 19706019
3. Mukkamala SK, Costa RA, Fung A, Sarraf D, Gallego-Pinazo R, Freund KB. Optical coherence tomographic imaging of sub-retinal pigment epithelium lipid. Arch Ophthalmol 2012;130:1-7. PMID 22892986
4. Christakopoulos C, Pryds A, Larsen M. Subretinal lamellar bodies in polypoidal choroidal vasculopathy. Acta Ophthalmol 2013;91:e248-9. PMID 23279931
5. Clemens CR, Krohne TU, Charbel Issa P, et al. High-resolution optical coherence tomography of subpigment epithelial structures in patients with pigment epithelium detachment secondary to age-related macular degeneration. Br J Ophthalmol 2012;96:1088-91. PMID 22694959
6. Garcia Filho CA, Yehoshua Z, Gregori G, Puliafito C, Rosenfeld PJ. Optical coherence tomography, Fifth ed. In: Ryan SJ, Schachat AP, Wilkinson CP, Hinton DR, Sadda S, Wiedemann P, editors. Retina. London: Elsevier, 2013.
7. Mrejen S, Sarraf D, Mukkamala SK, Freund KB. Multimodal imaging of pigment epithelial detachment: a guide to evaluation. Retina 2013;33:1735-62. PMID 23873168
8. Inoue M, Arakawa A, Yamane S, Kadonosono K. Imaging of sub-retinal pigment epithelial linear structures in patients with age-related macular degeneration. Eur J Ophthalmol 2014;24:744-50. PMID 24474382
9. Querques G, Georges A, Ben Moussa N, Sterkers M, Souied EH. Appearance of regressing drusen on optical coherence tomography in age-related macular degeneration. Ophthalmology 2014;121:173-9. PMID 23891523
10. Strouthidis NG, Grimm J, Williams GA, Cull GA, Wilson DJ, Burgoyne CF. A comparison of optic nerve head morphology viewed by spectral domain optical coherence tomography and by serial histology. Invest Ophthalmol Vis Sci 2010;51:1464-74. PMID 19875649
11. Litts KM, Messinger JD, Dellatorre K, Yannuzzi LA, Freund KB, Curcio CA. Clinicopathological correlation of outer retinal tubulation in age-related macular degeneration. JAMA Ophthalmol 2015;3/5/15 online. PMID 25742505
12. Walton KW, Dunkerley DJ. Studies on the pathogenesis of corneal arcus formation. II. Immunofluorescent studies on lipid deposition in the eye of the lipid-fed rabbit. J. Pathol. 1974;114:217-229. PMID 4141731

13. Schwenke DC, Behr SR. Vitamin E combined with selenium inhibits atherosclerosis in hypercholesterolemic rabbits independently of effects on plasma cholesterol concentrations. Circulation Research 1998;83:366-377. PMID 9721693
14. Ramírez AI, Salazar JJ, De Hoz R, et al. Macroglial and retinal changes in hypercholesterolemic rabbits after normalization of cholesterol levels. Exp Eye Res 2006;83:1423-38. PMID 17007836
15. Salazar JJ, Ramírez AI, de Hoz R, et al. Alterations in the choroid in hypercholesterolemic rabbits: Reversibility after normalization of cholesterol levels. Exp Eye Res 2006;84:412-22. PMID 17178413
16. Li C-M, Bradley K, Chung BH, Millican CL, Curcio CA. Absence of Bruch's membrane (BrM) cholesterol deposition in rabbits consuming atherogenic diets. ARVO Meeting Abstracts 2002;E-Abstract:2813. PMID n.a.